MAGNETISM

Accelerated discovery of new magnets in the Heusler alloy family

Stefano Sanvito,[1,2]* Corey Oses,[2,3] Junkai Xue,[2,3] Anurag Tiwari,[1†] Mario Zic,[1] Thomas Archer,[1] Pelin Tozman,[1] Munuswamy Venkatesan,[1] Michael Coey,[1] Stefano Curtarolo[2,3]*

Magnetic materials underpin modern technologies, ranging from data storage to energy conversion to contactless sensing. However, the development of a new high-performance magnet is a long and often unpredictable process, and only about two dozen magnets are featured in mainstream applications. We describe a systematic pathway to the design of novel magnetic materials, which demonstrates a high throughput and discovery speed. On the basis of an extensive electronic structure library of Heusler alloys containing 236,115 prototypical compounds, we filtered those displaying magnetic order and established whether they can be fabricated at thermodynamic equilibrium. Specifically, we carried out a full stability analysis of intermetallic Heusler alloys made only of transition metals. Among the possible 36,540 prototypes, 248 were thermodynamically stable but only 20 were magnetic. The magnetic ordering temperature, T_C, was estimated by a regression calibrated on the experimental T_C of about 60 known compounds. As a final validation, we attempted the synthesis of a few of the predicted compounds and produced two new magnets: Co_2MnTi, which displays a remarkably high T_C in perfect agreement with the predictions, and Mn_2PtPd, which is an antiferromagnet. Our work paves the way for large-scale design of novel magnetic materials at potentially high speed.

INTRODUCTION

Very few types of macroscopic order in condensed matter are as sensitive to details as magnetism. The magnetic interaction is usually based on the m-J paradigm, where localized magnetic moments, m, are magnetically coupled through the exchange interaction, J. Only a few elements in the periodic table can provide localized moments in the solid state, namely, $3d$ transition metals, $4f$ rare earths, and some $4d$ ions. Lighter $2p$ elements are prone to form close shells, whereas Hund's coupling is not strong enough to sustain a high-spin configuration in heavier elements [1]. The magnetic coupling then depends on how the wave functions of the magnetic ions overlap with each other, either directly, through other ions, or via delocalized electrons. This generates a multitude of mechanisms for magnetic coupling, operating at both sides of the metal/insulator transition boundary, and specific to the details of the chemical environment. In general, J is sensitive to the bond length, the bond angle, and the magnetic ion valence. It is thus not surprising that, among the ~100,000 unique inorganic compounds known to mankind [2], only about 2000 show magnetic order of any kind [3].

If one focuses on the magnets that are useful for consumer applications, then the choice becomes even more restricted, with no more than two dozens of compounds taking practically the entire global market. A useful magnet, regardless of the particular technology, should operate in the −50° to +120°C range, imposing the ordering temperature, T_C, to be at least 300°C. Specific technologies set additional constraints. Permanent magnets should display large magnetization and hysteresis [3]. Magnetic electrodes in high-performance tunnel junctions should grow epitaxially on a convenient insulator and have a band structure suitable for spin filtering [4]. If the same tunnel junction is used as spin-transfer torque magnetic memory element, then the magnet should also have a low Gilbert damping coefficient and a high Fermi-level spin polarization [4]. There are not many magnets matching all the criteria; hence, the design of a new magnet suitable for a target application is a complex and multifaceted task.

The search for a new magnet usually proceeds by trial and error, but the path may hide surprises. For instance, chemical intuition suggests that $SrTcO_3$ should be a poor magnet, because all $SrXO_3$ perovskites, with X in the chemical neighborhood of T_C, either are low-temperature magnetic (X = Ru, Cr, Mn, and Fe) or do not present any magnetic order (X = Mo). However, $SrTcO_3$ is a G-type antiferromagnet [5] with a remarkably high Néel temperature of 750°C, originating from a subtle interplay between p-d hybridization and Jahn-Teller distortion [6]. This shows that often a high-temperature magnet may represent a singularity in physical/chemical trends and that its search can defy intuition. For this reason, we take a completely different approach to the discovery process and demonstrate that a combination of advanced electronic structure theory and massive database creation and search, the high-throughput computational materials design approach [7], can provide a powerful tool for finding new magnetic materials.

Our computational strategy consists of three main steps. First, we construct an extensive database containing the computed electronic structures of potential novel magnetic materials, and we consider Heusler alloys (HAs) [8]. This extends to existing AFLOW.org set of repositories [9]. A rough stability analysis, based on evaluating the enthalpy of formation against reference single-phase compounds, provides a first screening of the database. However, this is not a precise measure of the thermodynamic stability of a material, because it does not consider decomposition into competing phases (single-element, binary, and ternary compounds). This analysis requires the computation of the enthalpy of formation of all possible decomposition members associated with the given Heusler compounds. This is our second step, and it is carried out only for intermetallic HAs, for which an extensive database is available [9]. Finally, we analyze the magnetic order of the predicted stable magnetic intermetallic HAs and, via a regression trained on available magnetic data, estimate their T_C. The theoretical screening is then validated by experimental synthesis of a few of the predicted compounds.

[1]School of Physics, AMBER and CRANN Institute, Trinity College, Dublin 2, Ireland. [2]Center for Materials Genomics, Duke University, Durham, NC 27708, USA. [3]Departments of Mechanical Engineering and Materials Science, Physics, and Chemistry, Duke University, Durham, NC 27708, USA.
*Corresponding author. Email: sanvitos@tcd.ie (S.S.); stefano@duke.edu (S.C.)
†Present address: Indian Institute of Technology, New Delhi, India.

We comment on the choice of the HAs. First, HA is a family of ternary compounds populated with several high-performance magnets (8), because many of them incorporate magnetic ions. Second, it is a rather large class that spans a wide variety of chemical compositions, giving us a large number of prototypes and a high chance of finding new compounds. Third, constructing a large library will allow us, at another time, to search for interesting material properties other than magnetism. Finally, most of the known magnetic HAs are metallic and they are well described by semilocal density functional theory (DFT), so we expect our method to be accurate.

RESULTS

The prototypical HA, X_2YZ (Cu$_2$MnAl-type), crystallizes in the $Fm\bar{3}m$ cubic space group, where the X atoms occupy the $8c$ Wyckoff position (1/4, 1/4, 1/4) and the Y and Z atoms are at the $4a$ (0, 0, 0) and $4b$ (1/2, 1/2, 1/2) positions, respectively. The crystal can be described as four interpenetrating face-centered cubic lattices, where the Y and Z atoms form an octahedral-coordinated rock-salt structure, whereas the X atoms occupy the tetrahedral voids (see Fig. 1A). Two alternative structures also exist. In the inverse Heusler (XY)XZ (Hg$_2$CuTi-type), the X and Z atoms form the rock-salt lattice, whereas the remaining X and Y atoms fill the tetrahedral sites (Fig. 1B); therefore, one X atom presents sixfold octahedral coordination and the other presents fourfold tetrahedral coordination. The second structure, the half Heusler XYZ (MgCuSb-type), is obtained by removing one of the X atoms, thus leaving a vacancy at one of the tetrahedral sites (Fig. 1C). The minimal unit cell describing all three types can be constructed as a tetrahedral $F\bar{4}3m$ cell, containing four (three for the case of the half Heusler) atoms (Fig. 1D). This cell allows for a ferromagnetic spin configuration and for a limited number of antiferromagnetic configurations.

We construct the HA library by considering all possible three-element combinations made of atoms from the 3d, 4d, and 5d periods and some elements from groups III to VI. In particular, we use Ag, Al, As, Au, B, Ba, Be, Bi, Br, Ca, Cd, Cl, Co, Cr, Cu, Fe, Ga, Ge, Hf, Hg, In, Ir, K, La, Li, Mg, Mn, Mo, Na, Nb, Ni, Os, P, Pb, Pd, Pt, Re, Rh, Ru, Sb, Sc, Se, Si, Sn, Sr, Ta, Tc, Te, Ti, Tl, V, W, Y, Zn, and Zr. Note that we have deliberately excluded rare earths, responding to the global need to design new magnets with a reduced rare earth content. Furthermore, we

have not imposed constraints on the total number of valence electrons (10, 11), because magnetism is found in a broad range of electron counts. For each combination of three elements (X, Y, and Z), all the possible regular, inverse, and half HAs are constructed, for a total of 236,115 prototypes. The electronic structure of all the prototypes is computed by DFT in the generalized gradient approximation (GGA) of the exchange correlation functional as parameterized by Perdew-Burke-Ernzerhof (12). Our DFT platform is the Vienna Ab initio Simulation Package (VASP) code (13), and each structure is fully relaxed. The typical convergence tolerance is 1 meV/atom, and this is usually achieved by sampling the Brillouin zone over a dense grid of 3000 to 4000 k-points per reciprocal atom. A much denser grid of 10,000 k-points is used for the static run to obtain accurate charge densities and density of states. The large volume of data is managed by the AFLOW code (14), which also generates the appropriate entries for the AFLOW database (9). Additional details about the computational method can be found in the study of Calderon et al. (15).

Let us begin our analysis by providing a broad overview of the database. A minimal criterion of stability for the 236,115 calculated compounds is that the enthalpy of formation of the X_2YZ structure, H_{X_2YZ}, is lower than the sum of the enthalpies of formation of its elementary constituents, namely, $\Delta H = H_{X_2YZ} - (2H_X + H_Y + H_Z) < 0$. This criterion returns us 35,602 compounds, where 6778 present a magnetic moment. Note that this number can be slightly underestimated because our unit cell may be different and incompatible with the magnetic cell, a priori unknown. This may result in the unit cell calculation to converge to a diamagnetic solution. In any case, this number is certainly significantly larger than the actual number of stable magnetic HAs. This can only be established by computing the entire phase diagram of each ternary compound, that is, by assessing the stability of any given X_2YZ structure against decomposition over all the possible alternative binary and ternary prototypes (for example, X_2YZ can decompose into $XY + XZ$, $X_2Y + Z$, and $XYZ + X$). This calculation is extremely intensive. An informative phase diagram for a binary alloy needs to be constructed over approximately 10,000 prototypes (16), which means that at least 30,000 calculations are needed for every ternary. As a consequence, mapping the stability of every calculated HA will require the calculation of approximately 15 million prototypes, which is quite a challenging task.

If the electronic structure and the enthalpy of formation of the relevant binaries are available, then one can construct the convex hull diagram for the associated ternary compounds (17). An example of this convex hull diagram for Al-Mn-Ni is shown in Fig. 1E. The figure shows that there is a stable phase, namely, Ni$_2$MnAl, with a formation energy of −404 meV/atom. In this case, there are also three other unstable ternary structures with $\Delta H < 0$, namely, Mn$_2$NiAl, NiMnAl, and Al$_2$MnNi. The enthalpy of formation of Mn$_2$NiAl is $\Delta H = -209$ meV/atom, and it is 121 meV/atom higher than tie plane, that of NiMnAl is −39 meV/atom (400 meV/atom above the tie plane), and that of Al$_2$MnNi is −379 meV/atom (100 meV/atom above the tie plane). This shows that $\Delta H < 0$ alone is not a stringent criterion for stability and that a full analysis needs to be performed before a call on a given ternary is made. Notably, Ni$_2$MnAl has been synthesized in a mixture of B2 and L2$_1$ phases (18), and it is a well-established magnetic shape memory alloy.

Given the enormous computational effort of mapping the stability of the entire database, we limited further analysis to intermetallic HAs made only with elements of the 3d, 4d, and 5d periods. These form a subset of the original 236,115 prototypes comprising 36,540 compounds, for which the corresponding binaries and known ternary
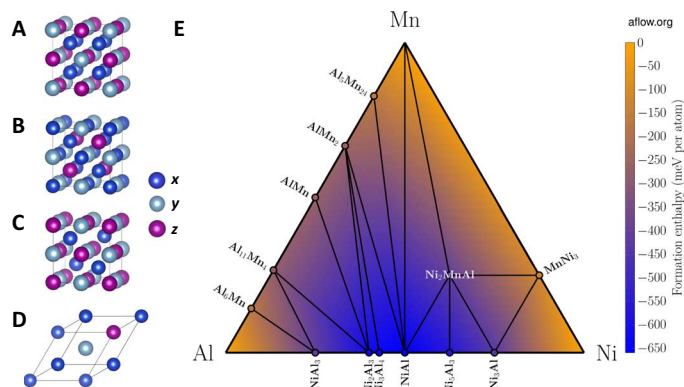
Fig. 1. Unit cells and phase stability of HAs. Possible HAs: (**A**) regular Heusler, (**B**) inverse Heusler, and (**C**) half Heusler. In (**D**), we show the unit cell used to construct the electronic structure database. (**E**) Ternary convex hull diagram for Al-Mn-Ni (note the presence of the stable HA, Ni$_2$MnAl).

energies are available in the AFLOW database (9). Our convex hull analysis thus establishes that, of the 36,540 compounds, only 248 are thermodynamically stable (see full list in the Supplementary Materials), among which 22 have a magnetic ground state compatible with the used unit cells (see Fig. 1D). Their calculated properties are presented in Table 1. Note that, in the last column of the table, we include an estimate of the robustness of a particular compound against decomposition, Δ^{30}.

A material is deemed as decomposable ("Y" in the table) if its enthalpy of formation is negative but <30 meV/atom lower than the most stable balanced decomposition. In contrast, a material is deemed robust ("N" in the table) when ΔH is >30 meV/atom away from that of the closest balanced decomposition. When this criterion is applied, we found that 14 of the predicted HAs can potentially decompose, whereas the other 8 are robust.

Table 1. Calculated properties of the 22 magnetic HAs found among all possible intermetallics. The table lists the unit cell volume of the $F\bar{4}3m$ cell, the c/a ratio for tetragonal cells (a), the Mn-Mn distance for Mn-containing alloys (d_{Mn-Mn}), the magnetic moment per formula unit (m), the spin polarization at the Fermi level (P_F), the enthalpy of formation (ΔH), the entropic temperature (T_S), and the magnetic ordering temperature (T_C). Note that T_C is evaluated only for Co_2YZ and X_2MnZ compounds for which a sufficiently large number of experimental data are available for other chemical compositions. In the case of Mn_2YZ compounds, we report the magnetic moment of the ground state and, in brackets, that of the ferromagnetic solution. The last column provides a more stringent criterion of stability. Δ^{30} = Y if the given compound has an enthalpy within 30 meV/atom from that of its most favorable balanced decomposition (potentially decomposable), and Δ^{30} = N if this enthalpy is >30 meV/atom lower (robust). f.u., formula unit.

Alloy	V (Å³)	c/a	a (Å)	d_{Mn-Mn} (Å)	m (μ_B/f.u.)	P_F	ΔH (eV/atom)	T_S (K)	T_C (K)	Δ^{30}
Mn₂PtRh	58.56		6.16	3.08	0.00 (9.05)	0.00 (0.86)	−0.29	3247	—	N
Mn₂PtCo	54.28		6.00	3.00	1.13 (9.04)	0.00 (0.86)	−0.17	1918	—	Y
Mn₂PtPd	60.75		6.24	3.12	0.00 (8.86)	0.00 (0.38)	−0.29	3218	—	N
Mn₂PtV	55.73		6.06	3.03	4.87 (4.87)	0.67	−0.30	3353	—	Y
Mn₂CoCr	47.19		5.73	2.87	4.84 (4.84)	0.02	−0.05	529	—	N
Co₂MnTi	49.68		5.84		4.92	0.58	−0.28	3122	940	N
Co₂VZn	46.87		5.73		1.01	0.93	−0.15	1653	228	Y
Co₂NbZn*	51.87	1.0	5.9		1.00	0.95	−0.18	2034	212	Y
Co₂NbZn	51.52	1.15	5.63		0.0	0.0	−0.20	2034	0	Y
Co₂TaZn*	51.80	1.0	5.92		0.98	0.63	−0.22	2502	125	N
Co₂TaZn	51.55	1.12	5.70		0.0	0.0	−0.23	2502	0	N
Rh₂MnTi	58.08		6.15	4.35	4.80	0.51	−0.58	6500	417	Y
Rh₂MnZr	64.50		6.37	4.50	4.75	0.34	−0.58	6518	338	Y
Rh₂MnHf	63.22		6.32	4.47	4.74	0.34	−0.67	7474	364	Y
Rh₂MnSc	61.62		6.27	4.43	4.31	0.77	−0.63	7031	429	N
Rh₂MnZn	54.95		6.03	4.27	3.37	0.63	−0.31	3444	372	Y
Pd₂MnAu*	64.21	1.0	6.36	4.49	4.60	0.06	−0.20	2203	853	Y
Pd₂MnAu	63.50	1.35	5.75	4.07	4.28	0.28	−0.33	2203	331	Y
Pd₂MnCu	57.63		6.13	4.34	4.53	0.06	−0.22	2492	415	Y
Pd₂MnZn*	58.88	1.0	6.17	4.37	4.33	0.38	−0.39	4399	894	Y
Pd₂MnZn	58.74	1.18	5.84	4.13	4.22	0.16	−0.47	4399	402	Y
Pt₂MnZn*	59.23	1.0	6.19	4.37	4.34	0.34	−0.45	5035	694	Y
Pt₂MnZn	58.95	1.22	5.79	4.10	4.13	0.02	−0.65	5035	381	Y
Ru₂MnNb	59.64		6.20	4.39	4.07	0.85	−0.19	2068	276	Y
Ru₂MnTa	59.72		6.20	4.39	4.06	0.86	−0.26	2912	305	N
Ru₂MnV	54.38		6.01	4.25	4.00	0.71	−0.16	1832	342	Y
Rh₂FeZn	54.60		6.02		4.24	0.49	−0.28	3150	—	N

*Not stable against tetragonal distortion (Co₂NbZn and Co₂TaZn become diamagnetic after distortion).

We further checked whether these magnetic ground states are stable against tetragonal distortion, which may occur in HAs, particularly with the Mn_2YZ composition. We found that the ground state of five prototypes, namely, Co_2NbZn, Co_2TaZn, Pd_2MnAu, Pd_2MnZn, and Pt_2MnZn, is tetragonally distorted. Furthermore, for two of them (Co_2NbZn and Co_2TaZn), the tetragonal distortion suppresses the magnetic order, indicating that the competition between the Stoner and band Jahn-Teller instability (19) favors a distorted nonmagnetic ground state. The analysis so far tells us that the incidence of stable magnetic HAs among the possible intermetallics is about 0.057%. When this is extrapolated to the entire database, we can forecast a total of about 140 stable magnetic alloys, of which about 60 are already known. In the same manner, we can estimate approximately 1450 stable nonmagnetic HAs, although this is just a crude forecast, because regions of strong chemical stability may be present in the complete database and absent in the intermetallic subset.

In Table 1, together with structural details, the magnetic moment per formula unit, m, and the enthalpy of formation, we report a few additional quantities that help us in understanding the potential of a given alloy as a useful magnet. The spin polarization of the density of state at the Fermi level $n_F^\sigma(\sigma = \uparrow, \downarrow)$ is calculated as (20)

$$P_F = \frac{n_F^\uparrow - n_F^\downarrow}{n_F^\uparrow + n_F^\downarrow}$$

and expresses the ability of a metal to sustain spin-polarized currents (21). We find a broad distribution of P_F's with values ranging from 0.93 (Co_2VZn) to 0.06 (Pd_2MnCu). None of the HAs display half-metallicity, and in general, their spin polarization is similar to that of the elementary $3d$ magnets (Fe, Co, and Ni). We then calculate the entropic temperature, T_S (7, 16, 22). For simplicity, we give the definition for an XY binary alloy, although all our calculations are performed for its ternary equivalent

$$T_s = \max_i \left[\frac{\Delta H \left(X_{x_i} Y_{1-x_i} \right)}{k_B [x_i \log x_i + (1 - x_i) \log (1 - x_i)]} \right]$$

where k_B is the Boltzmann constant and i counts all the stable compounds in the XY binary system. Effectively, T_S is a concentration-maximized formation enthalpy weighted by the inverse of its ideal entropic contribution (random alloy). It measures the ability of an ordered phase to resist deterioration into a temperature-driven, entropically promoted, disordered mixture. The sign of T_S is chosen such that a positive temperature is needed for competing against the compound stability (note that $T_S < 0$ if $\Delta H > 0$), and one expects $T_S \to 0$ for a compound spontaneously decomposing into a disordered mixture. If we analyze the T_S distribution for all the intermetallic HAs with $\Delta H < 0$ (8776 compounds), we find the behavior to closely follow that of a two-parameter Weibull distribution with a shape of 1.13 and a scale of 2585.63 (see histogram in the Supplementary Materials). The same distribution for the 248 stable intermetallic HAs is rather uniform in the range of 1000 to 10,000 K and presents a maximum at around 3500 K. A similar trend is observed for the 20 stable magnetic HAs, suggesting that several of them may be highly disordered.

Finally, Table 1 includes an estimate of the magnetic ordering temperatures, T_C. These were calculated on the basis of available experimental data. That is, we collected the experimental T_C's of approximately 40

known magnetic Heusler compounds (see the Supplementary Materials) and performed a linear regression correlating the experimental T_C's with a range of calculated electronic and structural properties, namely, equilibrium volume, magnetic moment per formula unit, spin decomposition, and number of valence electrons. The regression is possible only for those compounds for which the set of available experimental data is large enough, namely, for Co_2YZ and X_2MnZ HAs. We trained the regression over the existing data and found that, for the two classes Co_2YZ and X_2MnZ, the typical error in the T_C estimate is in the range of 50 K, which is taken as our uncertainty.

DISCUSSION

We found three different classes of stable magnetic HAs: Co_2YZ, X_2MnZ, and Mn_2YZ. In addition, we predicted that Rh_2FeZn is also stable. This is rather unique because there are no other HAs with Fe in octahedral coordination and no magnetic ions at the tetrahedral positions.

The first class is Co_2YZ, a class already populated by about 25 known compounds all lying on the Slater-Pauling curve (8). Our analysis reveals four new stable alloys: three of them (Co_2VZn, Co_2NbZn, and Co_2TaZn) have low valence electron counts of 25, and one (Co_2MnTi) presents the large count of 29. The regression correctly places these four on the Slater-Pauling curve (see Fig. 2) and predicts the remarkably high T_C of 940 K for Co_2MnTi. This is rather interesting because only about two dozen magnets are known to have a T_C in that range (3). Therefore, the discovery of Co_2MnTi has to be considered as exceptional. The other three new compounds in this class are all predicted to have a T_C of around 200 K, but two of them become nonmagnetic upon tetragonal distortion, leaving only Co_2VZn magnetic (T_C, ~228 K).
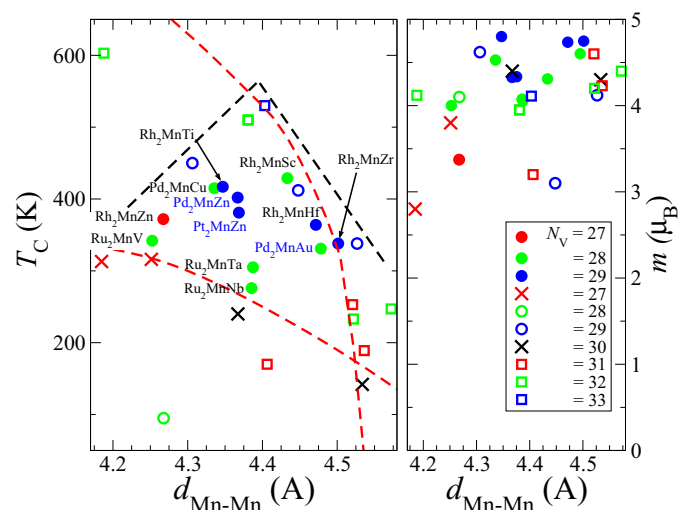
The second class is X_2MnZ, in which we find 13 new stable magnets, most of them including a $4d$ ion (Ru, Rh, and Pd) in the tetrahedral X position. In general, these compounds have a magnetic moment per
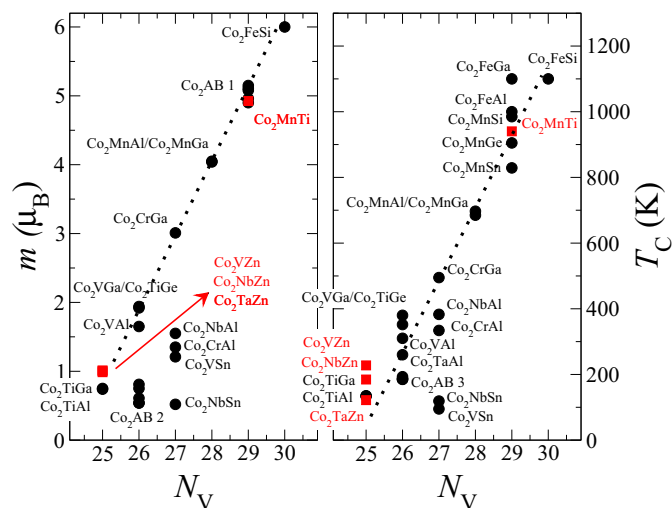
Fig. 2. Slater-Pauling curve for magnetic HAs of the Co₂YZ form. (**Left**) Magnetic moment per formula unit, m, plotted against the number of valence electron, N_V. (**Right**) T_C. Red symbols correspond to predicted HAs, whereas black symbols correspond to existing materials. For clarity, several compounds were named collectively: Co_2AB 1, Co_2FeGa, Co_2FeAl, Co_2MnSi, Co_2MnGe, and Co_2MnSn; Co_2AB 2, Co_2TaAl, Co_2ZrAl, Co_2HfAl, Co_2HfGa, and Co_2TaGa; Co_2AB 3, Co_2ZrAl, Co_2HfAl, Co_2HfGa, and Co_2TaGa.

formula unit ranging between 4 and 5 μ_B, consistent with the nominal 2+ valence of Mn in octahedral coordination. The regression, run against 18 existing compounds of which 13 are with X = Ru, Rh, or Pd, establishes a correlation between the Mn-Mn nearest neighbor distance, $d_{\text{Mn-Mn}}$, and T_C, as shown in Fig. 3.

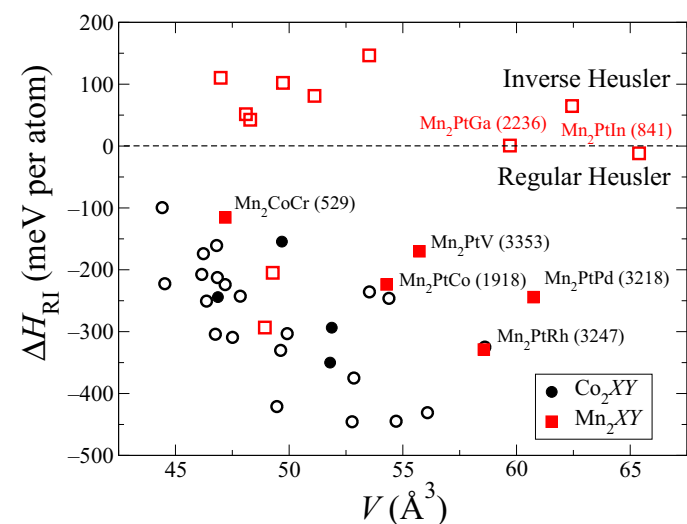We find that T_C is a nonmonotonic function of $d_{\text{Mn-Mn}}$ with a single maximum at $d_0 \sim 4.4$ Å, corresponding to a temperature of 550 K (the maximum coincides approximately with Cu$_2$MnSn). The only apparent exception to this trend is the prototypical Cu$_2$MnAl, which displays a large T_C and relatively small $d_{\text{Mn-Mn}}$ (23). A strong sensitivity of the T_C of Mn-containing compounds to $d_{\text{Mn-Mn}}$ was observed a long time ago and rationalized in an empirical T_C–$d_{\text{Mn-Mn}}$ curve by Castelliz (24). This predicts that T_C is not monotonically dependent on $d_{\text{Mn-Mn}}$ and has a maximum at around $d_{\text{Mn-Mn}} = 3.6$ Å. This curve has been validated for a number of HAs, and it has been used to explain the positive pressure coefficient of T_C, $(1/T_C)(dT_C/dP)$, found, for instance, in Rh$_2$MnSn (25). Refinements of the Castelliz curve predict that the rate of change of T_C with $d_{\text{Mn-Mn}}$ in HAs is related to the valence count (26), although the position of the maximum is not. In general, the results in Fig. 3, including several experimental data, seem to contradict this picture because a monotonically decreasing T_C is expected for any $d_{\text{Mn-Mn}} > 3.6$ Å, that is, practically for any HAs of the form X_2MnZ. There are a few possible reasons for this disagreement. First, the Castelliz curve assumes that only Mn carries a magnetic moment, which is unlikely because many of the X_2MnZ compounds in Fig. 3 have Rh or Pd in the X position, two highly spin-polarizable ions. Second, many HAs in Fig. 3 present various levels of disorder, meaning that Mn-Mn pairs separated by less than the nominal $d_{\text{Mn-Mn}}$ are likely to be present in actual samples. We thus propose that the trend in Fig. 3 (see dashed black lines) represents a new empirical curve, valid for X_2MnZ HAs and taking these effects into account.

The last class of predicted magnetic HAs is populated by Mn$_2$YZ compounds. These have recently received significant attention because of their high T_C and the possibility of displaying tetragonal distortion and hence large magnetocrystalline anisotropy (27). Experimentally, when the $4c$ position is occupied by an element from groups III, IV, or V, one finds the regular Heusler structure if the atomic number of the Y ion is smaller than that of Mn, $Z(Y) < Z(\text{Mn})$, and the inverse one for $Z(Y) > Z(\text{Mn})$. To date, only Mn$_2$VAl and Mn$_2$VGa have been grown with a Y element lighter than Mn so that, except those two, all other Mn$_2$YZ HAs crystallize with the inverse structure (see Fig. 4). In the case of the two regular HAs (Mn$_2$VAl and Mn$_2$VGa), the magnetic order is ferrimagnetic, with the two Mn ions at the tetrahedral sites being antiferromagnetically coupled to V (28–30). In contrast for the inverse Mn$_2$-based HAs, the antiferromagnetic alignment is between the two Mn ions, and the magnetic ground state thus depends on whether there are other magnetic ions in the compound. In general, however, site disorder is not uncommon (see the Supplementary Materials), and so is tetragonal distortion, so that the picture becomes more complicated. There are also some complex cases, such as that of Mn$_3$Ga, presenting a ground state with a noncollinear arrangement of both the spin and angular momentum (31).

If we now turn our attention to the predicted compounds, we find five stable compositions, of which three match the Δ^{30} robustness criterion. Most intriguingly, the regular $Fm\bar{3}m$ structure appears to be the ground state for all the compounds, regardless of their chemical composition. This sets Mn$_2$-based intermetallic compounds aside from those with elements from the main groups. In Fig. 4, we present the enthalpy of formation difference between the regular and the inverse structure, $\Delta H_{\text{RI}} = \Delta H_R - \Delta H_I$, for the computed and the experimentally known Mn$_2$-based HAs, together with their T_S and reference data for Co$_2$-based alloys. In general, we find that ΔH_{RI} for the Mn$_2$YZ class is significantly smaller than that for the Co$_2$YZ one. There are cases (for example, Mn$_2$PtGa and Mn$_2$PtIn) in which the two phases are almost

Fig. 3. Critical temperature and magnetic moment for X_2MnZ HAs. Magnetic data for X_2MnZ magnets: T_C (**left**) and magnetic moment per formula unit (**right**) as a function of the Mn-Mn distance, $d_{\text{Mn-Mn}}$. Note that the T_C is limited to about 550 K and peaks at a volume of about 60 Å^3. In contrast, the magnetic moment is approximately constant, with values in between 4 and 5 μ_B. Closed circles (with associated chemical compositions) correspond to the predicted compounds, whereas the other symbols correspond to experimental data. Different colors correspond to different number of valence electrons, N_V. Blue chemical formulas correspond to compounds displaying tetragonal distortion. The two red lines denote Castelliz-Kanomata curves, whereas the black line is meant to guide the eye.


Fig. 4. Enthalpy of formation difference between the regular and inverse Heusler structure, ΔH_{RI}, for Mn$_2$-containing compounds as a function of the cell volume. The solid red squares (with chemical formulas) are the predicted stable intermetallic materials, whereas the open red squares are existing compounds. For completeness, we also include data for Co$_2$-based HAs (open symbols, existing compounds; solid symbols, predicted compounds). In brackets beside the chemical formulas, we report the value for the entropic temperature, T_S, in kelvin.

degenerate, and different magnetic configurations can favor one over the other. Overall, one thus expects these compounds to be highly disordered. Finally, we take a look at the magnetic ground state. In all cases, the compounds present some degree of antiferromagnetic coupling, which results in either a zero-moment ground state when Mn is the only magnetic ion or a ferrimagnetic configuration when other magnetic ions are present.

The last step in our approach consisted of validating the theoretical predictions by experiments. We have attempted the synthesis of four HAs: Co_2MnTi, Mn_2PtPd, Mn_2PtCo, and Mn_2PtV. Co_2MnTi is chosen because of its predicted high T_C, whereas, among the Mn_2-based alloys, we have selected two presenting ferrimagnetic ground states (Mn_2PtCo and Mn_2PtV) and one meeting the stringent Δ^{30} robustness criterion (Mn_2PtPd). The alloys have been prepared by arc melting in high-purity Ar, where the ingots were remelted four times to ensure homogeneity. An excess of 3 weight % (wt %) Mn is added to compensate for Mn losses during arc melting (see the Supplementary Materials for details). Structural characterization was carried out by powder x-ray diffraction (XRD), whereas magnetic measurements were made using a superconducting magnetometer in a field of up to 5 T. Furthermore, the microstructure was analyzed by scanning electron microscopy of the polished bulk samples, whereas the compositions were determined by energy-dispersive x-ray (EDX) spectroscopy.

Two of the four HAs have been successfully synthesized (Co_2MnTi and Mn_2PtPd), whereas the other two (Mn_2PtCo and Mn_2PtV) decomposed into binary compounds (see the Supplementary Materials for details). In Fig. 5, we present the structural and magnetic characterization of Co_2MnTi. It crystallizes in a cubic structure related to the regular $Fm\bar{3}m$ Heusler structure, with no evidence of secondary phases and a lattice parameter of $a = 5.89$ Å, in close agreement with theory, $a = 5.84$ Å. The measured XRD pattern shows little intensity corresponding to the superstructure peaks, and we cannot exclude that the samples present a large degree of site disorder. This means that our crystallographic analysis is also compatible with a B2 (CsCl-type) or A2 (body-centered cubic) structure. The magnetization curve displays little temperature dependence and a saturation moment of 4.29 μ_B/f.u. at 4 K, consistent with the calculated ferromagnetic ground state (see Table 1). Notably, the T_C extrapolated from the zero-field cooled magnetization curve in a field of 1 T is found to be 938 K, essentially identical to that predicted by our regression, 940 K. Note that the regression calibrated to the experimental data, including disordered compounds, is largely controlled by the total number of valence electrons so that possible site-occupation disorder should affect little the prediction. This is a remarkable result, because it is the first time that a new high-temperature ferromagnet has been discovered by high-throughput means.

In addition, in the case of Mn_2PtPd, a single phase is found without evidence of decomposition. The XRD pattern (Fig. 6B) corresponds to a tetragonally distorted regular Heusler with space group $I4/mmm$ ($TiAl_3$-type) and lattice parameters $a = 4.03$ Å and $c = 7.24$ Å. Our magnetic data show a magnetic transition at ~320 K, which shifts to a slightly higher temperature upon field cooling (Fig. 6A). Magnetization curves at room temperature and 4 K show no hysteresis or spontaneous magnetization, indicating that the compound is antiferromagnetic at low temperature. From Table 1, it appears that the only difference between the calculated and experimental data for Mn_2PtPd concerns the tetragonal distortion. However, the search for tetragonal distortion reported in the table was performed only for the ferromagnetic state.
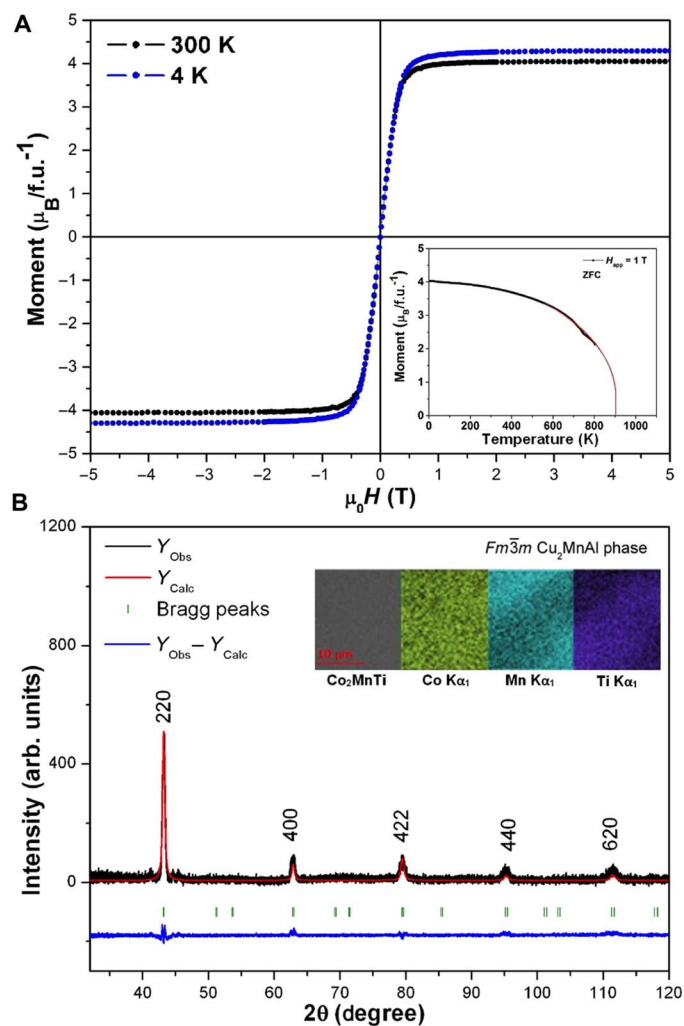
Fig. 5. Co_2MnTi. (**A**) Magnetization curve at 4 and 300 K [inset: zero-field cooled (ZFC) magnetization curve as a function of temperature in a magnetic field of 1 T]. (**B**) XRD spectrum (inset: EDX chemical composition analysis). Co_2MnTi crystallizes in a single $Fm\bar{3}m$ phase corresponding to a regular Heusler. The T_C extrapolated from the magnetization curve is around 900 K. arb. units, arbitrary units.

Further analysis of the antiferromagnetic ground state (see the Supplementary Materials) reveals that Mn_2PtPd is antiferromagnetic and tetragonally distorted, with a c/a ratio of around 1.3, in good agreement with experiments.

In conclusion, we have demonstrated a new systematic pathway to the discovery of novel magnetic materials. We have created an extensive library of Heusler compounds, including about 250,000 prototypes. For the subclass of intermetallic alloys, we have been able to establish the material stability against decomposition of 20 novel magnetic HAs belonging to the Co_2YZ, Mn_2YZ, and X_2MnZ classes. A simple machine learning method, correlating calculated microscopic electronic structure quantities with macroscopic measured properties, has been used to predict the magnetic T_C of these compounds. The method has been put to the test with the experimental synthesis of four compounds and validated by the growth of two. In particular, we have discovered a new high-temperature ferromagnet (Co_2MnTi) and a tetragonally distorted antiferromagnet (Mn_2PtPd). Our method offers a new high-throughput tool for the discovery of new magnets, which can now be applied to
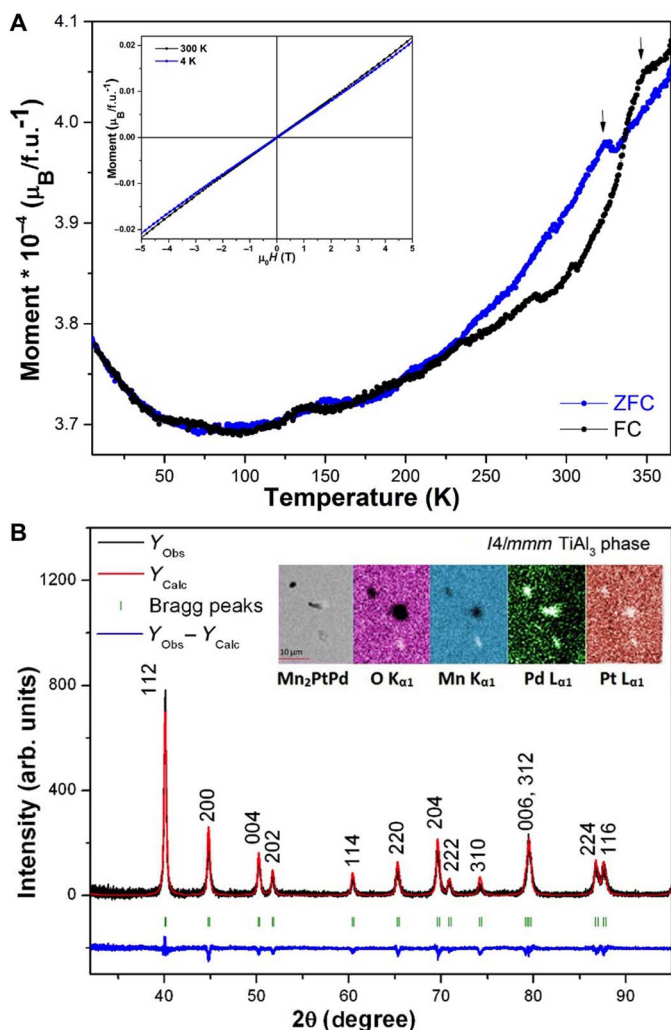
Fig. 6. Mn₂PtPd. (**A**) Field cooled and zero-field cooled magnetization curves as a function of temperature in a magnetic field of 0.1 T (inset: magnetization curve at 4 and 300 K). (**B**) XRD spectrum (inset: EDX chemical composition analysis). Mn₂PtPd crystallizes in a single *I4/mmm* (TiAl₃-type) phase corresponding to a regular tetragonal distorted Heusler. SEM images confirm that the bulk sample is mainly of Mn₂PtPd composition (gray color) with a small amount of secondary Mn-O inclusions, which have a spherical shape of 400 to 900 nm in diameter and do not appear in the XRD spectrum.

other structural families, opening new possibilities for designing materials for energy, data storage, and spintronic applications.

MATERIALS AND METHODS

The electronic structure of all the Heusler prototypes was computed by DFT in the GGA of the exchange correlation functional as parameterized by Perdew-Burke-Ernzerhof (*12*). Our DFT platform was the VASP code (*13*), and each structure was fully relaxed. The typical convergence tolerance was 1 meV/atom, and this was usually achieved by sampling the Brillouin zone over a dense grid of 3000 to 4000 *k*-points per reciprocal atom. A much denser grid of 10,000 *k*-points was used for the static run to obtain accurate charge densities and density of states. All calculations were performed by including spin polarization and were initialized from a ferromagnetic ground state. Additional antiferromagnetic initializations were considered in the case of the Mn₂-based HAs.

The large volume of data was managed by the AFLOW code (*14*), which also generated the appropriate entries for the AFLOW database (*9*).

The alloys were prepared by arc melting in high-purity Ar, with the ingots remelted four times to ensure homogeneity. An excess of 3 wt % Mn was added to compensate for Mn losses during arc melting (see the Supplementary Materials for details). Structural characterization was carried out by powder XRD, whereas magnetic measurements were made using a superconducting magnetometer in a field of up to 5 T. Furthermore, the microstructure was analyzed by scanning electron microscopy of the polished bulk samples, whereas the compositions were determined by EDX spectroscopy.

SUPPLEMENTARY MATERIALS

Supplementary material for this article is available at http://advances.sciencemag.org/cgi/content/full/3/4/e1602241/DC1

fig. S1. Magnetization curves for Mn₂PtCo.
fig. S2. Structural and chemical characterization of Mn₂PtCo.
fig. S3. Magnetization curves for Mn₂PtV.
fig. S4. Structural and chemical characterization of Mn₂PtV.
fig. S5. Histogram of the entropic temperature, T_S, for all the 8776 intermetallic HAs displaying negative enthalpy of formation ($\Delta H < 0$ and $T_S > 0$).
fig. S6. Histogram of the entropic temperature, T_S, for all the 248 intermetallic HAs estimated stable after the construction of the convex hull diagrams for the ternary phase.
fig. S7. Total energy as a function of the c/a ratio for Mn₂PtPd calculated with GGA-DFT.
References (*32–96*)

REFERENCES AND NOTES

1. J. F. Janak, Uniform susceptibilities of metallic elements. *Phys. Rev. B* **16**, 255–262 (1977).
2. FIZ Karlsruhe and NIST, Inorganic crystal structure database; http://icsd.fiz-karlsruhe.de/icsd/.
3. J. M. D. Coey, *Magnetism and Magnetic Materials* (Cambridge Univ. Press, 2010).
4. E. Y. Tsymbal, I. Žútíc, Eds., in *Handbook of Spin Transport and Magnetism* (CRC Press, 2012).
5. E. E. Rodriguez, F. Poineau, A. Llobet, B. J. Kennedy, M. Avdeev, G. J. Thorogood, M. L. Carter, R. Seshadri, D. J. Singh, A. K. Cheetham, High temperature magnetic ordering in the 4d perovskite SrTcO₃. *Phys. Rev. Lett.* **106**, 067201 (2011).
6. C. Franchini, T. Archer, J. He, X.-Q. Chen, A. Filippetti, S. Sanvito, Exceptionally strong magnetism in the 4d perovskites RTcO₃ (R = Ca, Sr, Ba). *Phys. Rev. B* **83**, 220402 (2011).
7. S. Curtarolo, G. L. W. Hart, M. B. Nardelli, N. Mingo, S. Sanvito, O. Levy, The high-throughput highway to computational materials design. *Nat. Mater.* **12**, 191–201 (2013).
8. T. Graf, C. Felser, S. S. P. Parkin, Simple rules for the understanding of Heusler compounds. *Prog. Solid State Chem.* **39**, 1–50 (2011).
9. S. Curtarolo, W. Setyawan, S. Wang, J. Xue, K. Yang, R. H. Taylor, L. J. Nelson, G. L. W. Hart, S. Sanvito, M. B. Buongiorno-Nardelli, N. Mingo, O. Levy, AFLOWLIB.ORG: A distributed materials properties repository from high-throughput ab initio calculations. *Comput. Mater. Sci.* **58**, 227–235 (2012).
10. X. Zhang, L. Yu, A. Zakutayev, A. Zunger, Sorting stable versus unstable hypothetical compounds: The case of multi-functional ABX half-Heusler filled tetrahedral structures. *Adv. Funct. Mater.* **22**, 1425–1435 (2012).
11. F. Yan, X. Zhang, Y. Y. G. Yu, L. Yu, A. Nagaraja, T. O. Mason, A. Zunger, Design and discovery of a novel half-Heusler transparent hole conductor made of all-metallic heavy elements. *Nat. Commun.* **6**, 7308 (2015).
12. J. P. Perdew, K. Burke, M. Ernzerhof, Generalized gradient approximation made simple. *Phys. Rev. Lett.* **77**, 3865–3868 (1996).
13. G. Kresse, J. Furthmuller, Efficiency of ab initio total energy calculations for metals and semiconductors using a plane-wave basis set. *Comput. Mater. Sci.* **6**, 15–50 (1996).
14. S. Curtarolo, W. Setyawan, G. L. W. Hart, M. Jahnatek, R. V. Chepulskii, R. H. Taylor, S. Wang, J. Xue, K. Yang, O. Levy, M. Mehl, D. Morgan, AFLOW: An automatic framework for high-throughput materials discovery. *Comput. Mater. Sci.* **58**, 218–226 (2012).
15. C. E. Calderon, J. J. Plata, C. Toher, C. Oses, O. Levy, M. Fornari, A. Natan, M. J. Mehl, G. L. W. Hart, M. B. Nardelli, S. Curtarolo, The AFLOW standard for high-throughput materials science calculations diagrams. *Comput. Mater. Sci.* **108**, 233–238 (2015).
16. G. L. W. Hart, S. Curtarolo, T. B. Massalski, O. Levy, Comprehensive search for new phases and compounds in binary alloy systems based on platinum-group metals, using a computational first-principles approach. *Phys. Rev. X* **3**, 041035 (2013).
17. H. L. Lukas, S. G. Fries, B. Sundman, *Computational Thermodynamics: The Calphad Method* (Cambridge Univ. Press, 2007).

18. K. R. A. Ziebeckt, P. J. Webster, Helical magnetic order in Ni₂MnAl. *J. Phys. F Met. Phys.* **5**, 1756–1766 (1975).

19. J. Labbé, J. Friedel, Instabilité électronique et changement de phase cristalline des composés du type V₃Si à basse température. *J. Phys. France* **27**, 153–165 (1966).

20. I. I. Mazin, How to define and calculate the degree of spin polarization in ferromagnets. *Phys. Rev. Lett.* **83**, 1427–1430 (1999).

21. J. M. D. Coey, S. Sanvito, Magnetic semiconductors and half-metals. *J. Phys. D Appl. Phys.* **37**, 988–993 (2004).

22. J. Yong, Y. Jiang, D. Usanmaz, S. Curtarolo, X. Zhang, J. Shin, L. Li, X. Pan, I. Tachuchi, R. L. Greene, Composition-spread growth and the robust topological surface state of Kondo insulator SmB₆ thin films. *Appl. Phys. Lett.* **105**, 222403 (2014).

23. D. P. Oxley, R. S. Tebble, K. C. Williams, Heusler alloys. *J. Appl. Phys.* **34**, 1362–1364 (1963).

24. L. Castelliz, Beitrag zum ferromagnetismus von legierungen der Übergangsmetalle mit elementen der B-gruppe. *Z. Metallk.* **46**, 198–203 (1955).

25. Y. Adachia, H. Morita, T. Kanomata, A. Sato, H. Yoshida, T. Kaneko, H. Nishihara, Pressure effect on the Curie temperature of the Heusler alloys Rh₂MnZ (Z = Sn, Ge). *J. Alloys Compd.* **383**, 37–39 (2004).

26. T. Kanomata, K. Shirakawa, T. Kaneko, Effect of hydrostatic pressure on the Curie temperature of the Heusler alloys Ni₂MnZ (Z = Al, Ga, In, Sn and Sb). *J. Magn. Magn. Mater.* **65**, 76–82 (1987).

27. G. Kreiner, A. Kalache, S. Hausdorf, V. Alijani, J.-F. Qian, G. Shan, U. Burkhardt, S. Ouardi, C. Felser, New Mn₂-based Heusler compounds. *Z. Anorg. Allg. Chem.* **640**, 738–752 (2014).

28. T. Nakamichi, C. V. Stager, Phenomenological formula of NMR satellite of Heusler alloys and magnetic structure of Mn₂VAl. *J. Magn. Magn. Mater.* **31–34**, 85–87 (1983).

29. H. Itoh, T. Nakamichi, Y. Yamaguchi, N. Kazama, Neutron diffraction study of Heusler type alloy Mn₀.₄₇V₀.₂₈Al₀.₂₅. *Trans. Jpn. Inst. Met.* **24**, 265–271 (1983).

30. K. R. Kumar, N. H. Kumar, G. Markandeyulu, J. A. Chelvane, V. Neu, P. D. Babu, Structural, magnetic and transport properties of half-metallic ferrimagnet Mn₂VGa. *J. Magn. Magn. Mater.* **320**, 2737–2740 (2008).

31. K. Rode, N. Baadji, D. Betto, Y.-C. Lau, H. Kurt, M. Venkatesan, P. Stamenov, S. Sanvito, J. M. D. Coey, E. Fonda, E. Otero, F. Choueikani, P. Ohresser, F. Porcher, G. André, Site-specific order and magnetism in tetragonal Mn₃Ga thin films. *Phys. Rev. B* **87**, 184429 (2013).

32. J. Kübler, G. H. Fecher, C. Felser, Understanding the trend in the Curie temperatures of Co₂-based Heusler compounds: Ab initio calculations. *Phys. Rev. B* **76**, 024414 (2007).

33. J. Webster, K. R. A. Ziebeck, in *Alloys and Compounds of d-Elements with Main Group Elements, Part 2*, H. R. J. Wijn, Ed. (Springer, 1988).

34. T. Sasaki, T. Kanomata, T. Narita, H. Nishihara, R. Note, H. Yoshida, T. Kaneko, Magnetic properties of Co₂TiGa compound. *J. Alloys Compd.* **317**, 406–410 (2001).

35. J. Barth, G. H. Fecher, B. Balke, T. Graf, A. Shkabko, A. Weidenkaff, P. Klaer, M. Kallmayer, H.-J. Elmers, H. Yoshikawa, S. Ueda, K. Kobayashi, C. Felser, Anomalous transport properties of the half-metallic ferromagnets Co₂TiSi, Co₂TiGe and Co₂TiSn. *Philos. Trans. R. Soc. A* **369**, 3588–3601 (2011).

36. W. Zhang, Z. Qian, Y. Sui, Y. Liu, W. Su, M. Zhang, Z. Liu, G. Liu, G. Wu, Magnetism and Hall effect of the Heusler alloy Co₂ZrSn synthesized by melt-spinning process. *J. Magn. Magn. Mater.* **299**, 255–259 (2006).

37. T. Kanomata, Y. Chieda, K. Endo, H. Okada, M. Nagasako, K. Kobayashi, R. Kainuma, R. Y. Umetsu, H. Takahashi, Y. Furutani, H. Nishihara, K. Abe, Y. Miura, M. Shirai, Magnetic properties of the half-metallic Heusler alloys Co₂VGa. *Phys. Rev. B* **82**, 144415 (2010).

38. H. C. Kandpal, G. H. Fecher, C. Felser, Calculated electronic and magnetic properties of the half-metallic, transition metal based Heusler compounds. *J. Phys. D Appl. Phys.* **40**, 1507 (2007).

39. T. Kanomata, T. Sasaki, H. Nishihara, H. Yoshida, T. Kaneko, S. Hane, T. Goto, N. Takeishi, S. Ishida, Magnetic properties of ferromagnetic Heusler alloy Co₂ZrAl. *J. Alloys Compd.* **393**, 26–33 (2005).

40. A. U. B. Wolter, A. Bosse, D. Baabe, I. Maksimov, D. Mienert, H. H. Klauß, F. J. Litterst, D. Niemeier, R. Michalak, C. Geibel, R. Feyerherm, R. Hendrikx, J. A. Mydosh, S. Süllow, Structure and magnetic order of the Heusler compound Co₂NbSn. *Phys. Rev. B* **66**, 174428 (2002).

41. M. Hakimi, P. Kameli, H. Salamati, Structural and magnetic properties of Co₂CrAl Heusler alloys prepared by mechanical alloying. *J. Magn. Magn. Mater.* **322**, 3443–3446 (2010).

42. A. D. Svyazhin, E. I. Shreder, V. I. Voronin, I. F. Berger, S. E. Danilov, Atomic disorder and the magnetic, electrical, and optical properties of a Co₂CrAl Heusler alloy. *JETP* **116**, 452–459 (2013).

43. S. Trudel, O. Gaier, J. Hamrle, B. Hillebrands, Magnetic anisotropy, exchange and damping in cobalt-based full-Heusler compounds: An experimental review. *J. Phys. D Appl. Phys.* **19**, 193001 (2010).

44. A. W. Carbonari, R. N. Saxena, W. Pendl Jr., J. Mestnik-Filho, R. N. Atilli, M. Olzon-Dionysio, S. D. de Souza, Magnetic hyperfine field in the Heusler alloys Co₂YZ (Y = V, Nb, Ta, Cr; Z = Al, Ga). *J. Magn. Magn. Mater.* **163**, 313–321 (1996).

45. H. Wijn, *Magnetic Properties of Metals: d-Elements, Alloys and Compounds* (Springer-Verlag, 1991).

46. P. Klaer, M. Kallmayer, H. J. Elmers, L. Basit, J. Thöne, S. Chadov, C. Felser, Localized magnetic moments in the Heusler alloy Rh₂MnGe. *J. Phys. D Appl. Phys.* **42**, 084001 (2009).

47. J. C. Suits, New magnetic compounds with Heusler and Heusler-related structures. *Phys. Rev. B* **14**, 4131–4135 (1976).

48. F. A. Hames, J. Crangle, Ferromagnetism in Heusler-type alloys based on platinum-group or palladium-group metals. *J. Appl. Phys.* **42**, 1336–1338 (1971).

49. B. R. Coles, W. Hume-Rothery, H. P. Myers, The structure and properties of the alloy Cu₂MnIn. *Proc. R. Soc. A* **196**, 125 (1949).

50. P. J. Webster, R. S. Tebble, Magnetic and chemical order in Pd₂MnAl in relation to order in the Heusler alloys Pd₂MnIn, Pd₂MnSn, and Pd₂MnSb. *J. Appl. Phys.* **39**, 471 (1968).

51. C. C. M. Campbell, T. Birchall, J. C. Suits, A study of Sn and Fe site hyperfine fields in ferromagnetic metals including the Rh-based Heusler alloys. *J. Phys. F Met. Phys.* **7**, 727–743 (1977).

52. P. J. Websterand, R. S. Tebble, The magnetic and chemical ordering of the Heusler alloys Pd₂MnIn, Pd₂MnSn and Pd₂MnSb. *Philos. Mag.* **16**, 347–361 (1967).

53. G. E. Bacon, E. W. Mason, The magnetic structures of the alloys Au₂(Mn,Al)₂. *Proc. Phys. Soc.* **92**, 713–725 (1967).

54. G. E. Bacon, J. S. Plant, Magnetic order in the AuMn alloy derivatives Au₂(Mn,Z)₂ where Z is Al, Cu, Ga, In or Zn. *J. Phys. F* **3**, 2003 (1973).

55. T. Kanomata, M. Kikuchi, H. Yamauchi, Magnetic properties of Heusler alloys Ru₂MnZ (Z = Si, Ge, Sn and Sb). *J. Alloys Compd.* **414**, 1–7 (2006).

56. M. Gotoh, M. Ohashi, T. Kanomata, Y. Yamaguchi, Spin reorientation in the new Heusler alloys Ru₂MnSb and Ru₂MnGe. *Phys. B Condens. Matter* **213–214**, 306–308 (1995).

57. K. H. J. Buschow, P. G. van Engen, Magnetic and magneto-optical properties of Heusler alloys based on aluminium and gallium. *J. Magn. Magn. Mater.* **25**, 90–96 (1981).

58. C. Jiang, M. Venkatesan, J. M. D. Coey, Transport and magnetic properties of Mn₂VAl: Search for half-metallicity. *Solid State Commun.* **118**, 513–516 (2001).

59. Note that the tetragonal phase is obtained when annealing at 400°C. A higher annealing temperature of 800°C results in a disorder pseudocubic phase. No magnetic data are available for this second phase.

60. T. Gasi, A. K. Nayak, J. Winterlik, V. Ksenofontov, P. Adler, M. Nicklas, C. Felser, Exchange-spring like magnetic behavior of the tetragonal Heusler compound Mn₂FeGa as a candidate for spin-transfer torque. *Appl. Phys. Lett.* **102**, 202402 (2013).

61. Note that Mn₂NiGa is a shape memory alloy, displaying a martensitic transformation at a critical temperature T_m = 270 K. The structure is cubic for $T > T_m$ and tetragonal for $T < T_m$.

62. G. D. Liu, J. L. Chen, Z. H. Liu, X. F. Dai, G. H. Wu, B. Zhang, X. X. Zhang, Martensitic transformation and shape memory effect in a ferromagnetic shape memory alloy: Mn₂NiGa. *Appl. Phys. Lett.* **87**, 262504 (2005).

63. G. D. Liu, X. F. Dai, S. Y. Yu, Z. Y. Zhu, J. L. Chen, G. H. Wu, H. Zhu, J. Q. Xiao, Physical and electronic structure and magnetism of Mn₂NiGa: Experiment and density-functional theory calculations. *Phys. Rev. B* **74**, 054435 (2006).

64. P. J. Brown, T. Kanomata, K. Neumann, K. U. Neumann, B. Ouladdiaf, A. Sheikh, K. R. A. Ziebeck, Atomic and magnetic order in the shape memory alloy Mn₂NiGa. *J. Phys. Condens. Matter* **22**, 506001 (2010).

65. A. K. Nayak, M. Nicklas, S. Chadov, C. Shekhar, Y. Skourski, J. Winterlik, C. Felser, Large zero-field cooled exchange-bias in bulk Mn₂PtGa. *Phys. Rev. Lett.* **110**, 127204 (2013).

66. A. K. Nayak, M. Nicklas, C. Shekhar, C. Felser, Kinetic arrest related to a first-order ferrimagnetic to antiferromagnetic transition in the Heusler compound Mn₂PtGa. *Appl. Phys. Lett.* **113**, 17E308 (2013).

67. A. K. Nayak, M. Nicklas, S. Chadov, P. Khuntia, C. Shekhar, A. Kalache, M. Baenitz, Y. Skourski, V. K. Guduru, A. Puri, U. Zeitler, J. M. D. Coey, C. Felser, Design of compensated ferrimagnetic Heusler alloys for giant tunable exchange bias. *Nat. Mater.* **14**, 679–684 (2015).

68. V. Alijani, J. Winterlik, G. H. Fecher, C. Felser, Tuning the magnetism of the Heusler alloys Mn₃₋ₓCoₓGa from soft and half-metallic to hard-magnetic for spin-transfer torque applications. *Appl. Phys. Lett.* **99**, 222510 (2011).

69. M. Meinert, J.-M. Schmalhorst, C. Klewe, G. Reiss, E. Arenholz, T. Böhnert, K. Nielsch, Itinerant and localized magnetic moments in ferrimagnetic Mn₂CoGa thin films probed by x-ray magnetic linear dichroism: Experiment and ab initio theory. *Phys. Rev. B* **84**, 132405 (2011).

70. T. Hori, M. Akimitsu, H. Miki, K. Ohoyoama, Y. Yamaguchi, Magnetic properties of (Mn₁₋ₓRuₓ)₃Ga alloys. *Appl. Phys. A* **74**, S737–S739 (2002).

71. H. Kurt, K. Rode, P. Stamenov, M. Venkatesan, Y.-C. Lau, E. Fonda, J. M. D. Coey, Cubic Mn₂Ga thin films: Crossing the spin gap with ruthenium. *Phys. Rev. Lett.* **112**, 027201 (2014).

72. L. Yang, B. Liu, F. Meng, H. Liu, H. Luo, E. Liu, W. Wang, G. Wu, Magnetic properties of Heusler alloy Mn₂RuGe and Mn₂RuGa ribbons. *J. Magn. Magn. Mater.* **379**, 1–5 (2015).

73. A. K. Nayak, C. Shekhar, J. Winterlik, A. Gupta, C. Felser, Mn₂PtIn: A tetragonal Heusler compound with exchange bias behavior. *Appl. Phys. Lett.* **100**, 152404 (2012).

74. H. Luo, P. Jia, G. Liu, F. Meng, H. Liu, E. Liu, W. Wang, G. Wu, Martensitic transformation in Heusler alloy Mn₂PtIn: Theoretical and experimental investigation. *Solid State Commun.* **170**, 44–47 (2013).

75. The ground-state magnetic configuration is noncollinear with a canting angle between the two inequivalent magnetic ions of 180 ± 55°.

76. V. Alijani, O. Meshcheriakova, J. Winterlik, G. Kreiner, G. H. Fecher, C. Felser, Increasing Curie temperature in tetragonal Mn₂RhSn Heusler compound through substitution of Rh by Co and Mn by Rh. *J. Appl. Phys.* **110**, 063904 (2013).

77. O. Meshcheriakova, S. Chadov, A. K. Nayak, U. K. Rößler, J. Kübler, G. André, A. A. Tsirlin, J. Kiss, S. Hausdorf, A. Kalache, W. Schnelle, M. Nicklas, C. Felser, Large noncollinearity and spin reorientation in the novel Mn₂RhSn Heusler magnet. *Phys. Rev. Lett.* **113**, 087203 (2014).

78. K. Endo, T. Kanomata, H. Nishihara, K. R. A. Ziebeck, Magnetic properties of new compounds RuMn₂Sn and RuMn₂Si. *J. Alloys Compd.* **510**, 1–5 (2012).

79. S. Ouardi, G. H. Fecher, C. Felser, J. Kübler, Realization of spin gapless semiconductors: The Heusler compound Mn₂CoAl. *Phys. Rev. Lett.* **110**, 100401 (2013).

80. M. E. Jamer, B. A. Assaf, T. Devakul, D. Heiman, Magnetic and transport properties of Mn₂CoAl oriented films. *Appl. Phys. Lett.* **103**, 142403 (2013).

81. Y. J. Zhang, G. J. Li, E. K. Liu, J. L. Chen, W. H. Wang, G. H. Wu, Ferromagnetic structures in Mn₂CoGa and Mn₂CoAl doped by Co, Cu, V, and Ti. *J. Appl. Phys.* **113**, 123901 (2013).

82. The T_C is evaluated from the theory of Meinert et al. (*83*).

83. M. Meinert, J.-M. Schmalhorst, G. Reiss, Exchange interactions and Curie temperatures of Mn₂CoZ compounds. *J. Phys. Condens. Matter* **23**, 116005 (2011).

84. G. D. Liu, X. F. Dai, H. Y. Liu, J. L. Chen, Y. X. Li, G. Xiao, G. H. Wu, Mn₂CoZ (Z = Al, Ga, In, Si, Ge, Sn, Sb) compounds: Structural, electronic, and magnetic properties. *Phys. Rev. B* **77**, 014424 (2008).

85. N. Lakshmi, A. Pandey, K. Venugopalan, Hyperfine field distributions in disordered Mn₂CoSn and Mn₂NiSn Heusler alloys. *Bull. Mater. Sci.* **25**, 309–313 (2002).

86. J. Winterlik, G. H. Fecher, B. Balke, T. Graf, V. Alijani, V. Ksenofontov, C. A. Jenkins, O. Meshcheriakova, C. Felser, G. Liu, S. Ueda, K. Kobayashi, T. Nakamura, M. Wójcik, Electronic, magnetic, and structural properties of the ferrimagnet Mn₂CoSn. *Phys. Rev. B* **83**, 174448 (2011).

87. X. Dai, G. Liu, L. Chen, J. Chen, G. Wu, Mn₂CoSb compound: Structural, electronic, transport and magnetic properties. *Solid State Commun.* **140**, 533–537 (2006).

88. R. B. Helmholdt, K. H. J. Buschow, Crystallographic and magnetic structure of Ni₂MnSn and NiMn₂Sn. *J. Less Common Met.* **128**, 167–171 (1987).

89. H. Luo, G. Liu, Z. Feng, Y. Li, L. Ma, G. Wu, X. Zhu, C. Jiang, H. Xu, Effect of the main-group elements on the electronic structures and magnetic properties of Heusler alloys Mn₂NiZ (Z=In, Sn, Sb). *J. Magn. Magn. Mater.* **321**, 4063–4066 (2009).

90. H. Luo, F. Meng, Z. Feng, Y. Li, W. Zhu, G. Wu, X. Zhu, C. Jiang, H. Xu, Ferromagnetism in the Mn-based Heusler alloy Mn₂NiSb. *J. Appl. Phys.* **105**, 103903 (2009).

91. J. Winterlik, B. Balke, G. H. Fecher, C. Felser, M. C. M. Alves, F. Bernardi, J. Morais, Structural, electronic, and magnetic properties of tetragonal Mn₃₋ₓGa: Experiments and first-principles calculations. *Phys. Rev. B* **77**, 054406 (2008).

92. E. Krén, G. Kádár, K. Pál, J. Sólyom, P. Szabó, T. Tarnóczi, Magnetic structures and exchange interactions in the Mn-Pt system. *Phys. Rev.* **171**, 574–585 (1968).

93. J. S. Kouvel, Exchange anisotropy in cobalt-manganese alloys. *J. Phys. Chem. Solids* **16**, 107–114 (1960).

94. M. Matsui, T. Ido, K. Sato, K. Adachi, Ferromagnetism and antiferromagnetism in Co–Mn alloy. *J. Phys. Soc. Jpn.* **28**, 791 (1970).

95. A. Z. Men'shikov, G. A. Takzei, Y. A. Dorofeev, V. A. Kazantsev, A. K. Kostyshin, I. I. Sych, The magnetic phase diagram of cobalt-manganese alloys. *J. Exp. Theor. Phys.* **62**, 734 (1985).

96. A. F. Andresen, A. Kjekshus, R. Møllerud, W. B. Pearson, Equiatomic transition metal alloys of manganese. V. On the magnetic properties of the PtMn phase. *Acta Chem. Scand.* **20**, 2529–2534 (1966).

Science Advances

Accelerated discovery of new magnets in the Heusler alloy family

Stefano SanvitoCorey OsesJunkai XueAnurag TiwariMario ZicThomas ArcherPelin TozmanMunuswamy VenkatesanMichael CoeyStefano Curtarolo

View the article online
https://www.science.org/doi/10.1126/sciadv.1602241
Permissions
https://www.science.org/help/reprints-and-permissions

Use of this article is subject to the Terms of service